



**HAL**  
open science

# **$\beta$ -Damascenone Highly Diluted in Hydroalcoholic Mixtures: Phase Equilibrium Measurements, Thermodynamic Modeling, and Simulation of a Batch Distillation**

Gabriela Zanghelini, Martine Esteban-Decloux, Stéphane Vitu, Pierre Giampaoli, Violaine Athès

## ► To cite this version:

Gabriela Zanghelini, Martine Esteban-Decloux, Stéphane Vitu, Pierre Giampaoli, Violaine Athès.  $\beta$ -Damascenone Highly Diluted in Hydroalcoholic Mixtures: Phase Equilibrium Measurements, Thermodynamic Modeling, and Simulation of a Batch Distillation. *Industrial and engineering chemistry research*, 2022, 61 (49), pp.18127-18137. 10.1021/acs.iecr.2c01755 . hal-03883202

**HAL Id: hal-03883202**

**<https://hal.science/hal-03883202v1>**

Submitted on 2 Dec 2022

**HAL** is a multi-disciplinary open access archive for the deposit and dissemination of scientific research documents, whether they are published or not. The documents may come from teaching and research institutions in France or abroad, or from public or private research centers.

L'archive ouverte pluridisciplinaire **HAL**, est destinée au dépôt et à la diffusion de documents scientifiques de niveau recherche, publiés ou non, émanant des établissements d'enseignement et de recherche français ou étrangers, des laboratoires publics ou privés.

# **$\beta$ -Damascenone highly diluted in hydroalcoholic mixtures: phase equilibrium measurements, thermodynamic modeling and simulation of a batch distillation**

Gabriela Zanghelini<sup>a\*</sup>, Martine Esteban-Decloux<sup>a</sup>, Stéphane Vitu<sup>a,b</sup>, Pierre Giampaoli<sup>a</sup> and Violaine Athès<sup>a</sup>

<sup>a</sup>Université Paris-Saclay, INRAE, AgroParisTech, UMR SayFood, 91120 Palaiseau, France

<sup>b</sup>CNAM, 75003 Paris, France

\*Email: gabriela.zanghelini@agroparistech.fr

## **ABSTRACT**

$\beta$ -Damascenone is a carotenoid-derived compound that plays a key role in the characteristic aroma of wines and distilled spirits. Despite the valuable contribution of this compound to the flavor quality of alcoholic beverages, little is known about its volatility and its vapor-liquid equilibrium behavior in hydroalcoholic mixtures of different compositions. Such information is essential to be able to choose the right thermodynamic model for  $\beta$ -damascenone when using a distillation process simulation software to gain a better understanding of the behavior of  $\beta$ -damascenone during spirit distillation. In this context, this work presents new experimental VLE data for  $\beta$ -damascenone highly diluted in ethanol + water mixtures. The measurements were carried out in a recirculation ebulliometer operating at 101.3 kPa for ethanol mass fractions between (0.10 and 0.79) g·g<sup>-1</sup>. Activity coefficient model NRTL was used to correlate the experimental data and binary interaction parameters. The parameters obtained for the NRTL model were employed to simulate a laboratory-scale batch distillation of a model solution of  $\beta$ -damascenone, ethanol and water. The simulation results were well fitted to experimental data. This approach can be further extended to other compounds that contribute to the aroma of distilled spirits and the results can be transferred to simulate larger scale distillations.

**Keywords:** vapor-liquid equilibrium; batch distillation; simulation;  $\beta$ -damascenone; NRTL; alcoholic beverages.

## 1. INTRODUCTION

Spirit distillation holds the triple role of concentrating volatile aroma compounds from a fermented medium into an ethanol-rich distillate, selecting specific aroma fractions and generating new aroma compounds via chemical reactions<sup>1</sup>. Despite their extremely low concentrations in the hydroalcoholic matrix (with mass fractions between  $10^{-10}$  and  $10^{-3}$ ), aroma compounds play a primary role in the intricate aroma typicality of distilled beverages. The contribution of each compound to the overall aroma is dictated by intrinsic factors such as their partition between the hydroalcoholic matrix and the headspace, as well as physical, chemical and structural properties of the different components in the system and the interactions between them<sup>2</sup>. Thence, achieving a desired aroma bouquet in a spirit requires fine-tuning its composition in aroma compounds, which in turn entails controlling the distillation step.

Thermodynamically, alcoholic spirits can be approached as non-ideal multicomponent mixture of aroma compounds highly diluted in an ethanol – water solution. During distillation, compound separation is assured by deviations from a state of vapor-liquid equilibrium (VLE) prompted by a continuous addition of energy through heat. The thermal properties of the system are dictated by the two major components, ethanol and water, whereas the behavior of the minor components in the hydroalcoholic mixture throughout distillation depends on their pure compound properties, i.e., vapor pressure and enthalpy of vaporization, as well as activity coefficients at different ethanol – water compositions, which lead to different volatility values depending on the composition.

Aroma compounds in distilled spirits belong to several chemical families, namely alcohols, esters, carboxylic acids, norisoprenoids, terpenes, aldehydes and ketones. Amongst these families, norisoprenoids are a class of highly odorant carotenoid-derived compounds that greatly contribute to the varietal aroma of wine<sup>3,4</sup> and are often listed among the most odorant components in distilled spirits. Within norisoprenoids,  $\beta$ -damascenone is a particularly potent odorant, with odor thresholds as low as  $0.002 \mu\text{g}\cdot\text{L}^{-1}$  in water<sup>5</sup>,  $7 \mu\text{g}\cdot\text{L}^{-1}$  in wine<sup>6</sup> and  $0.05$  and  $10 \mu\text{g}\cdot\text{L}^{-1}$  in model ethanol-water solutions at, respectively, 12% v/v ethanol<sup>7</sup> and 40% v/v ethanol<sup>8</sup>. It is a natural component of grape which has been reported to impart fruity, apple-like notes in various wines, where it can be found in its free form or

bound to glycosylated moieties at concentrations between 0.1 and 10  $\mu\text{g}\cdot\text{L}^{-1}$ <sup>9</sup>. Moreover, distillation has been shown to substantially increase the concentrations of  $\beta$ -damascenone, likely prompted by the high temperatures and acidic conditions involved in the process<sup>10-14</sup>. As a result, and given its aforementioned low odor thresholds,  $\beta$ -damascenone is listed amongst the key odorants responsible for the characteristic aroma of rum<sup>15,16</sup>, apricot and apple distillates<sup>17</sup>, spine grape spirit<sup>18</sup>, whisky<sup>19</sup>, tequila<sup>20,21</sup>, cachaça<sup>22</sup>, cognac<sup>23,24</sup> and calvados<sup>25</sup>, and is thought to act as an aroma enhancer in wine<sup>7,26</sup> and distilled spirits such as cognac<sup>27</sup>. In light of the above, reaching a better understanding of how the distillation operation affects the behavior of  $\beta$ -damascenone would be valuable to gain a better control of the final aroma of a distilled spirit.

Process simulation software are promising tools to understand, design and optimize distillation processes for alcoholic spirits. It has been consistently applied over the years to represent industrial scale continuous distillations of cachaça<sup>28</sup>, neutral alcohol<sup>29-32</sup>, armagnac<sup>33</sup> and whisky<sup>34</sup>, as well as batch distillations of cognac<sup>35</sup>, bitter orange distillate<sup>32</sup>, cachaça<sup>36-38</sup>, pisco pear distillate<sup>39</sup> and fruit spirits<sup>40</sup>. The accurate simulation of a distillation process requires physical, chemical and thermodynamic pure component properties, as well as vapor-liquid equilibrium data for the different components in the system coupled to a suitable thermodynamic model<sup>30</sup>. While VLE data can often be obtained from extensive databases integrated in the simulation packages or from the literature, they are seldom available for multicomponent systems, particularly in dilute conditions<sup>41</sup>. A fast and cost-efficient alternative could be to employ predictive contribution methods such as UNIFAC, although the reliability and applicability of this approach can be limited for aqueous mixtures and multicomponent systems including highly diluted compounds<sup>42,43</sup>. A more reliable, albeit time-consuming alternative is to experimentally measure VLE data using static or dynamic methods.

Despite the averred importance of norisoprenoids and particularly  $\beta$ -damascenone in the sector of alcoholic beverages, only a scant amount of information concerning its thermodynamic properties is available in the literature and no VLE data for the system  $\beta$ -damascenone + ethanol + water have been reported to date. Furthermore, predictive methods such as UNIFAC are not readily applicable to  $\beta$ -damascenone since certain

elementary groups required to decompose the molecule are missing from the UNIFAC matrix. Therefore, the acquisition of experimental VLE data for  $\beta$ -damascenone in hydroalcoholic media would be valuable to get a better understanding of its behavior during spirit distillation and, particularly, to be able to represent the compound in computer simulation modules.

In light of the above, this work focuses on the experimental measurement of VLE data for  $\beta$ -damascenone highly diluted in ethanol + water mixtures at 101.3 kPa. Measurements were conducted in a recirculation ebulliometer for ethanol mass fractions between (0.10 and 0.79) g.g<sup>-1</sup> and equilibrium compositions were quantified by gas chromatography and densimetry. The experimental data were correlated by activity coefficient model NRTL and binary interaction parameters determined for the model. The reliability of the NRTL parameters to accurately simulate the behavior of  $\beta$ -damascenone during a distillation was tested by simulating laboratory-scale batch distillation of a model solution of  $\beta$ -damascenone, ethanol and water and comparing simulation results to experimental data.

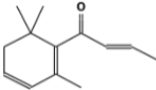
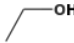
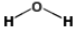
## 2. EXPERIMENTAL PROCEDURE

Employing process simulation software to accurately predict the behavior of  $\beta$ -damascenone during alcoholic distillations entails several different steps, which are explored in this section: (1) compilation of pure component properties, (2) measurement of vapor-liquid equilibrium data, (3) data correlation by thermodynamic models and (4) design of process simulation modules and (5) experimental validation.

### 2.1. Materials

The different components employed in the experiments are listed in Table 1 with their respective specifications and pure component properties. Deionized water (resistivity 18.2 M $\Omega$ -cm at 25 °C) obtained from a Milli-Q purification system was used throughout the experimental work. For simplification, the isomer (*E*)- $\beta$ -damascenone employed in the experiments will be referred to in the text as  $\beta$ -damascenone.

**Table 1.** Specifications and physical properties of the aroma compounds used in this work: molecular weight (MM/g·mol<sup>-1</sup>), normal boiling point ( $T_b$ /K) at 101.3 kPa, log<sub>10</sub> of the octanol/water partition coefficient at T = 298.15 K (log  $K_{ow}$ ).

| Compound               | (E)- $\beta$ -damascenone   | ethanol   | water   |
|------------------------|---|---|---|
| CAS number             | 23696-85-7  | 64-17-5   | 7732-18-5   |
| Formula                | C <sub>13</sub> H <sub>18</sub> O   | C <sub>2</sub> H <sub>6</sub> O   | H <sub>2</sub> O  |
| Structure              |  |  |  |
| Supplier               | Sigma-Aldrich   | Carlo Erba  |   |
| Mass fraction purity   | ≥0.992 <sup>a</sup>   | ≥0.999 <sup>a</sup>   |   |
| MM/g·mol <sup>-1</sup> | 190.28  | 46.07   | 18.01   |
| $T_b$ /K               | Exp.  | 351.45 <sup>b</sup>   | 373.15 <sup>b</sup>   |
|                        | Lit.  | 351.44 <sup>d,e,f</sup>   | 373.15 <sup>d,e,f</sup>   |
| log $K_{ow}$           | 4.20 <sup>g</sup>   | -0.31 <sup>h</sup>  | -1.38 <sup>h</sup>  |

<sup>a</sup>determined by gas chromatography by the supplier.

<sup>b</sup>This work, measured at 101.3 kPa ( $u(T_b) = 0.2$  K,  $u(P) = 0.5$  kPa). <sup>c</sup>Fonseca et al.<sup>44</sup>.

<sup>d</sup>Arce et al.<sup>45</sup>. <sup>e</sup>Kamihama et al.<sup>46</sup>. <sup>f</sup>Riddick et al.<sup>47</sup> <sup>g</sup>PhysProp database<sup>48</sup>. <sup>h</sup>Hansch et al.<sup>49</sup>.

## 2.2. Pure component properties

Modeling and simulation of chemical processes in commercial software generally requires models for temperature-dependent properties such as vapor pressure, enthalpy of vaporization and heat capacity. For water and ethanol, such data were promptly available in the database of the software Simulis Thermodynamics (ProSim SA, France)<sup>50</sup>, which was employed in this work for the thermodynamic modeling and the process simulation. For  $\beta$ -damascenone, which was missing from the database, pure component properties were gathered from the literature or predicted using group contribution methods, and the compound was subsequently added to the Simulis Thermodynamics database.

The saturated vapor pressure ( $P_i^0$ /Pa) of a pure compound  $i$  at a temperature  $T$ /K was calculated from the Antoine equation:

$$P_i^0(T)/\text{Pa} = \exp\left(A_i - \frac{B_i}{T/K + C_i}\right) \#(1)$$

in which  $A_i$ ,  $B_i$  and  $C_i$  are empirical coefficients specific to each compound.

The Antoine coefficients employed for the components in this work are listed in Table 2. For  $\beta$ -damascenone, the coefficients were determined by regression of experimental data measured by Nelson (2018)<sup>51</sup>.

**Table 2.** Antoine coefficients for calculating the vapor pressures of each component in the mixture at a given temperature using eq 1.  $T_{\min}/\text{K}$  and  $T_{\max}/\text{K}$  define the temperature interval in which the equation coefficients are valid.

| Compound             | $A_i$   | $B_i$   | $C_i$    | $T_{\min}/\text{K}$ | $T_{\max}/\text{K}$ | Source        |
|----------------------|---------|---------|----------|---------------------|---------------------|---------------|
| $\beta$ -damascenone | 21.13   | 4261.91 | -85.1995 | 298.15              | 450                 | <sup>51</sup> |
| ethanol              | 23.8046 | 3803.98 | -41.68   | 270                 | 369                 | <sup>52</sup> |
| water                | 23.1963 | 3816.44 | -46.13   | 284                 | 441                 | <sup>52</sup> |

The enthalpy of vaporization ( $\Delta H_{vap}/\text{J}\cdot\text{mol}^{-1}$ ) for  $\beta$ -damascenone at a temperature  $T/\text{K}$  was obtained from:

$$\Delta H_{vap} = -b_1 + b_2T \quad \#(2)$$

in which empirical coefficients  $b_1$  and  $b_2$  were set to -87749.66 and -80.56 (Fonseca et al., 2021<sup>44</sup>).

Temperature-dependent heat capacity ( $C_p/\text{J}\cdot\text{mol}^{-1}\cdot\text{K}^{-1}$ ) of liquid  $\beta$ -damascenone was predicted using the group contribution method proposed by Joback and Reid (1987)<sup>53</sup>:

$$C_p = A - 37.93 + [B + 0.210]T + [C - 3.91 \cdot 10^{-4}]T^2 + [D + 2.06 \cdot 10^{-7}]T^3 \quad \#(3)$$

With  $A = -49.26$ ,  $B = 1.20$ ,  $C = -8.12 \cdot 10^{-4}$  and  $D = 2.42 \cdot 10^{-7}$ .

For ethanol and water, models for  $\Delta H_{vap}$  and  $C_p$  values from the DIPPR database available in the ProSim suite were employed.

### 2.3. Vapor-liquid equilibrium of $\beta$ -damascenone in hydroalcoholic mixtures

This subsection describes the apparatus and methodology used for the VLE measurements of  $\beta$ -damascenone highly diluted in ethanol-water mixtures and the thermodynamic model employed to correlate the experimental data.

### 2.3.1. Experimental VLE measurements

The vapor-liquid equilibrium measurements were conducted in a glass Gillespie-type ebulliometer (Labodest VLE 602, iFisher GmbH, Germany) operating at isobaric and adiabatic conditions. System pressure is assessed by a digital manometer with an accuracy of  $\pm 0.5$  kPa (P-10 WIKA, iFisher GmbH, Germany) and the temperature of the coexisting liquid and vapor phases is measured in the separation chamber by a Pt-100 platinum probe with an accuracy of  $\pm 0.05$  K, periodically calibrated against a reference temperature probe (Pt-100 RTD 712, Fluke, France). A schematic diagram of the ebulliometer is provided in Figure 1. A validation procedure of our apparatus was conducted beforehand by measuring the binary ethanol-water at 101.3 kPa and assessing the thermodynamic consistency of the data, as described by Zanghelini et al. (2022)<sup>54</sup>.

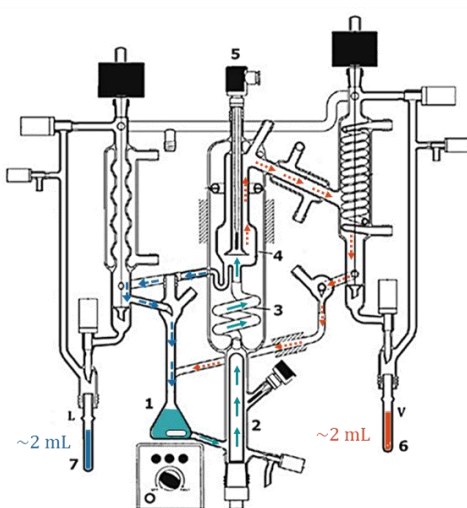


**Figure 1.** Schematic diagram of the Labodest VLE 602 (iFischer) apparatus: (1) mixing chamber, (2) reboiler, (3) “Cottrell pump” or equilibrium chamber, (4) separation chamber, (5) Pt-100 temperature probe, sampling tubes for the (6) vapor and (7) liquid phases. The arrows indicate the sense of circulation: (straight teal arrow), vapor-liquid; (dotted orange arrow), vapor; (dashed blue arrow), liquid.

The initial solutions consisted of  $\beta$ -damascenone, ethanol and water, with mass concentrations of  $\beta$ -damascenone from  $w_{\beta d} = (6.5 \cdot 10^{-4} \text{ to } 8.9 \cdot 10^{-4}) \text{ g} \cdot \text{g}^{-1}$  (or from  $x_{\beta d} = (8.0 \cdot 10^{-5} \text{ to } 1.6 \cdot 10^{-4})$  in mole fractions) and ethanol mass fractions ranging from  $w_{\text{Et}} = (0.10 \text{ to } 0.79) \text{ g} \cdot \text{g}^{-1}$ , which corresponds to a mole composition of  $x_{\text{Et}} = (0.04 \text{ to } 0.60)$ . The apparatus works by continuously circulation of the coexisting vapor and liquid phases until a state of thermodynamic equilibrium, as detailed by Zanghelini et al. (2022)<sup>54</sup>. At this point, a small



amount of sample (2 mL) is collected for the liquid and the condensed vapor through the sampling tubes (6,7) and kept under refrigeration for analysis of the equilibrium compositions. The term *vapor phase* employed in the figures and tables of this section thus corresponds to the vapor phase after condensation. The apparatus was fully rinsed between experiments by circulating pure ethanol.

### 2.3.2. Determination of equilibrium compositions

Ethanol concentrations in the liquid and condensed vapor samples were determined from density measurements conducted at 20 °C in an Anton Paar oscillating tube density meter (DMA 4500 M, Anton Paar) with a resolution of ( $\pm 0.00001$ ) g·cm<sup>-3</sup>. A two-point calibration of the device was performed regularly using pure degassed water and air. The calculations of ethanol mass fractions from density at a given temperature were based on the alcoholometric tables from the International Organization of Legal Metrology (OIML)<sup>55</sup>. The accuracy of the density measurements and of the ethanol mass concentrations determined using the OIML equation were assessed beforehand by measuring the densities of ethanol-water mixtures of known compositions comprising the entire composition range and confronting the measured values with the literature<sup>54</sup>.

The concentrations of  $\beta$ -damascenone in the vapor and liquid phases were measured in a gas chromatograph (GC Trace 1300 Series, Thermo Fisher Scientific) equipped with a flame ionization detector and an automatic sampler (TriPlus RSH, Thermo Fisher Scientific). The samples were adjusted to an ethanol mass fraction of  $w_{Et} = 0.6$  prior to analysis to minimize measurement variability between the different samples. All analyses were conducted in triplicate and  $\beta$ -ionone (CAS number 79-77-6; Sigma) was used as the internal standard at a fixed concentration of  $4.8 \cdot 10^{-3}$  g·g<sup>-1</sup> in an ethanol-water mixture at  $w_{Et} = 0.6$  g·g<sup>-1</sup>. For each analysis, an aliquot of 0.5  $\mu$ L of sample was directly injected in splitless mode using a 1  $\mu$ L precision glass syringe. Both inlet and detector temperatures were set to 250 °C. Helium was used as the carrier gas with a constant flow of 1.2 mL·min<sup>-1</sup>. Hydrogen and air flow for the flame jet were respectively 35 and 350 mL·min<sup>-1</sup>. The stationary phase was a ZB-Wax Plus capillary column (30 m x 0.32 mm, 0.5  $\mu$ m). The initial oven temperature was initially set to 80 °C and maintained for 2 min, then increased at a linear rate of 20 °C·min<sup>-1</sup> to 240 °C and

held for 5 min. The total running time was 15 min. The chromatographic data were acquired and analyzed using Chromeleon CDS software version 7.2.10 (Thermo Scientific). Quantification was based on calibration curves of the pure standard. Measurement uncertainties  $u$  were computed according to the GUM guidelines<sup>56,57</sup>. The detection and quantitation limits for  $\beta$ -damascenone estimated from the calibration curve were  $2.6 \cdot 10^{-5} \text{ g} \cdot \text{g}^{-1}$  and  $8.0 \cdot 10^{-5} \text{ g} \cdot \text{g}^{-1}$ , respectively (or  $3.9 \cdot 10^{-6}$  and  $1.2 \cdot 10^{-5}$  in mole fraction).

### 2.3.3. Thermodynamic modeling

The equilibrium condition entails an equality of temperatures, pressures and fugacities between the coexisting phases of saturated vapor and liquid. Given the low pressure of the VLE measurements (101.3 kPa), the vapor phase can be adequately described by the ideal gas law and the standard state liquid fugacity can be expressed as a function of pressure-independent activity coefficients<sup>58</sup>. The equilibrium data can thus be represented by a modified Raoult's law:

$$y_i P = \gamma_i(T, \mathbf{x}) x_i P_i^0(T) \quad \#(4)$$

in which  $P/\text{kPa}$  is the equilibrium pressure of the system,  $y_i$  and  $x_i$  are, respectively, vapor and liquid equilibrium mole fractions of component  $i$ ,  $\gamma_i$  is the activity coefficient of  $i$  in the liquid phase and  $P_i^0/\text{kPa}$  is the vapor pressure of pure component  $i$ , calculated from eq 1.

In spirit distillation, the behavior of an aroma compound (AC) between a liquid and a vapor phase at equilibrium is described by two properties derived from eq. 1: its absolute volatility or partition coefficient ( $K_{AC}$ ), which explains its distribution between the two phases, and its volatility relative to ethanol ( $\alpha_{AC/Et}$ ), as expressed by eqs. 5 and 6, respectively.

$$K_{AC} = \frac{y_{AC}}{x_{AC}} = \frac{\gamma_{AC}(T, \mathbf{x}) P_{AC}^0(T)}{P} \quad \#(5)$$

$$\alpha_{AC/Et} = \frac{K_{AC}}{K_{Et}} = \frac{y_{AC}/x_{AC}}{y_{Et}/x_{Et}} \quad \#(6)$$

Pressure-independent activity coefficients were calculated in this work using NRTL (Non-Random Two-Liquid), a semi-empirical model that has been consistently employed for

correlating ternary and multicomponent systems of aroma compounds highly diluted in hydroalcoholic mixtures<sup>59-61</sup>. The non-random intermolecular interactions within the mixture are accounted by adjustable binary interaction parameters that are fitted to the experimental data. The model includes two sets of adjustable parameters,  $A_{ij}^0$  and  $A_{ij}^T$ , and the non-randomness parameter  $\alpha_{ij}$ , which was set to 0.30 for all binaries as recommended in the literature for ethanol-water mixtures<sup>62</sup>.

For the binary ethanol (2) + water (3), interaction parameters were set to values from Puentes et al. (2018)<sup>60</sup> reported in Table 3. They have been consistently employed by our team for ternary systems involving aroma compounds in hydroalcoholic mixtures with proven reliability. For the binaries  $\beta$ -damascenone (1) + ethanol (2) and  $\beta$ -damascenone (1) + water (3), temperature-dependent parameters  $A_{ij}^T/\text{J}\cdot\text{mol}^{-1}\cdot\text{K}^{-1}$  and  $A_{ji}^T/\text{J}\cdot\text{mol}^{-1}\cdot\text{K}^{-1}$  are set to zero. Parameters  $A_{ij}^0$  and  $A_{ji}^0$  were determined from the experimental data using the software Simulis Thermodynamics<sup>50</sup> and Excel Solver by minimizing the following objective function:

$$OF = \sum_{i=1}^N \left( \frac{K_{i\beta d_{\text{exp}}} - K_{i\beta d_{\text{calc}}}}{K_{i\beta d_{\text{exp}}}} \right)^2 \#(7)$$

in which  $K_{i\beta d_{\text{exp}}}$  and  $K_{i\beta d_{\text{calc}}}$  are, respectively, the absolute volatilities of  $\beta$ -damascenone determined from the experimental data using eq. 5 and calculated with the NRTL model. The values for  $K_{i\beta d_{\text{calc}}}$  were calculated using the bubble point algorithm of Simulis Thermodynamics, which calculates vapor phase composition ( $\mathbf{y}$ ) and saturated liquid temperature ( $T$ ) from liquid phase composition ( $\mathbf{x}$ ) and system pressure ( $P$ ).

**Table 3.** Binary interaction parameters for the subsystem ethanol (2) + water (3)<sup>a</sup>.

| Binary (i-j) | $A_{23}^0/\text{J}\cdot\text{mol}^{-1}$ | $A_{32}^0/\text{J}\cdot\text{mol}^{-1}$ | $A_{23}^T/\text{J}\cdot\text{mol}^{-1}\cdot\text{K}^{-1}$ | $A_{32}^T/\text{J}\cdot\text{mol}^{-1}\cdot\text{K}^{-1}$ | $\alpha_{ij}$ |
|--------------|---|---|---|---|---------------|
| (2) – (3)    | 142.44                                  | 3559.28                                 | -7.53   | 23.63   | 0.3           |

<sup>a</sup>from Puentes et al.<sup>60</sup>

## 2.4. Simulation of batch distillation

This segment presents a computer simulation for a laboratory scale batch distillation that was carried out to assess the capability of the adjusted NRTL binary interaction parameters determined for the system to simulate the behavior of  $\beta$ -damascenone during a hydroalcoholic distillation.

### 2.4.1. Experimental setup

The experimental batch distillations were conducted for the ternary mixture in an Oldershaw-type glass distillation column (Vasse) composed of two thermally insulated column sections with five perforated plates each. The columns are connected at the bottom to a reboiler consisting of a triple neck round bottom flask with a volume capacity of 2 L and a 500 W heating mantle with an experimentally determined power of 375 W measured for pure water. A schematic representation of the apparatus is displayed in Figure 2. The temperature of the boiling liquid throughout the distillation process was measured by a Pt 100 temperature probe inserted in the flask and pressure drop was assessed by a water-column manometer connected to the reboiler. Reflux and sampling were controlled by a magnetic solenoid valve whose opening (sampling) and closing (reflux) were regulated by a control unit.



time and their composition was measured as described in subsection 2.3.2. Heat losses were calculated from preliminary runs with pure water and/or pure ethanol.

#### **2.4.2. Simulation procedure**

The simulation module for the laboratory-scale batch distillation was implemented using the software BatchColumn version 1.4.36.0 (ProSim SA, France). The temperature-dependent vapor pressures, enthalpies of vaporization and heat capacities for  $\beta$ -damascenone were computed using the models detailed in section 2.2. For ethanol and water, pure component properties were calculated using models from the DIPPR database available in the ProSim suite. The vapor-liquid equilibrium approach previously described, and the binary interaction parameters determined in this study were employed for the simulation.

### **3. RESULTS AND DISCUSSION**

#### **3.1. Vapor-liquid equilibrium**

Experimental VLE data were measured at 101.3 kPa for  $\beta$ -damascenone highly diluted in ethanol + water mixtures with ethanol concentrations between (0.10 and 0.79) g.g<sup>-1</sup>. The equilibrium composition of each phase for the 16 different mixtures is reported in Table 4 in terms of mole fractions. The corresponding saturated vapor pressures, partition coefficients, relative volatilities and activity coefficients for  $\beta$ -damascenone are listed in Table 5.

**Table 4.** Experimental VLE data for  $\beta$ -damascenone ( $\beta$ d) highly diluted in ethanol (Et) + water (w) mixtures. With  $T/\text{K}$ , equilibrium temperature;  $\rho/\text{g}\cdot\text{cm}^{-3}$ , density of the mixture in the liquid (L) and condensed vapor (V) phases at 293.15 K;  $\mathbf{x}$  and  $\mathbf{y}$ , mole compositions of the liquid and vapor phase, respectively, and  $u(x_{\beta\text{d}})$  and  $u(y_{\beta\text{d}})$  the standard uncertainties for  $\beta$ -damascenone.

| $T/\text{K}$ | $\rho_{\text{L}}/\text{g}\cdot\text{cm}^{-3}$ | $x_{\text{Et}}$ | $10^5 x_{\beta\text{d}}$ | $10^5 u(x_{\beta\text{d}})$ | $\rho_{\text{V}}/\text{g}\cdot\text{cm}^{-3}$ | $y_{\text{Et}}$ | $10^5 y_{\beta\text{d}}$ | $10^5 u(y_{\beta\text{d}})$ |
|--------------|---|-----------------|--------------------------|-----------------------------|---|-----------------|--------------------------|-----------------------------|
| 365.4        | 0.9861  | 0.029           | 7.132                    | 0.027                       | 0.9157  | 0.276           | 107.954                  | 0.218                       |
| 365.3        | 0.9847  | 0.033           | 7.619                    | 0.027                       | 0.9144  | 0.282           | 132.825                  | 0.262                       |
| 363.1        | 0.9808  | 0.045           | 8.330                    | 0.027                       | 0.8967  | 0.349           | 86.003                   | 0.168                       |
| 363.1        | 0.9792  | 0.050           | 8.946                    | 0.028                       | 0.8985  | 0.342           | 86.390                   | 0.160                       |
| 361.3        | 0.9759  | 0.062           | 9.873                    | 0.028                       | 0.8860  | 0.393           | 60.202                   | 0.104                       |
| 361.3        | 0.9751  | 0.065           | 9.686                    | 0.027                       | 0.8847  | 0.399           | 57.426                   | 0.096                       |
| 360.6        | 0.9734  | 0.071           | 7.976                    | 0.023                       | 0.8802  | 0.419           | 35.547                   | 0.074                       |
| 360.0        | 0.9708  | 0.081           | 8.967                    | 0.025                       | 0.8765  | 0.435           | 31.954                   | 0.065                       |
| 358.0        | 0.9600  | 0.121           | 11.986                   | 0.028                       | 0.8666  | 0.483           | 16.421                   | 0.024                       |
| 357.9        | 0.9587  | 0.126           | 11.936                   | 0.027                       | 0.8643  | 0.494           | 14.252                   | 0.021                       |
| 356.7        | 0.9480  | 0.164           | 10.528                   | 0.026                       | 0.8597  | 0.518           | 8.284                    | 0.014                       |
| 356.6        | 0.9456  | 0.172           | 10.851                   | 0.026                       | 0.8579  | 0.527           | 7.428                    | 0.013                       |
| 355.7        | 0.9287  | 0.229           | 14.563                   | 0.028                       | 0.8530  | 0.555           | 9.783                    | 0.016                       |
| 355.0        | 0.9171  | 0.269           | 11.182                   | 0.024                       | 0.8498  | 0.573           | 5.585                    | 0.012                       |
| 355.0        | 0.9149  | 0.277           | 11.234                   | 0.024                       | 0.8496  | 0.574           | 5.302                    | 0.012                       |
| 352.5        | 0.8468  | 0.591           | 18.453                   | 0.028                       | 0.8295  | 0.698           | 1.905                    | 0.017                       |

The other standard uncertainties are  $u(T) = 0.2 \text{ K}$ ,  $u(P) = 0.5 \text{ kPa}$ ,  $u(\rho_{\text{L}}) = u(\rho_{\text{V}}) = 0.0002 \text{ g}\cdot\text{cm}^{-3}$ ,  $u(T_{\rho}) = 0.03 \text{ K}$ ,  $u(x_{\text{Et}}) = u(y_{\text{Et}}) = 0.004$ .

**Table 5.** Experimental VLE variables describing the behavior of  $\beta$ -damascenone ( $\beta$ d) highly diluted in hydroalcoholic mixtures at  $P = 101.3$  kPa. With  $T/\text{K}$ , equilibrium temperature;  $x_{\text{Et}}$ , ethanol mole fractions in the liquid phase;  $P_{\beta\text{d}}^0/\text{kPa}$ , saturated vapor pressure of  $\beta$ -damascenone;  $K_{\beta\text{d}}$  and  $K_{\text{Et}}$ , partition coefficient of  $\beta$ -damascenone and ethanol, respectively;  $\alpha_{\beta\text{d}/\text{Et}}$ , relative volatility of  $\beta$ -damascenone in relation to ethanol;  $\gamma_{\beta\text{d}}$ , activity coefficient of  $\beta$ -damascenone.

| $T/\text{K}$ | $x_{\text{Et}}$ | $P_{\beta\text{d}}^0/\text{kPa}$ | $K_{\beta\text{d}}$ | $K_{\text{Et}}$ | $\alpha_{\beta\text{d}/\text{Et}}$ | $\log \gamma_{\beta\text{d}}$ |
|--------------|-----------------|----------------------------------|---------------------|-----------------|------------------------------------|-------------------------------|
| 365.4        | 0.029           | 0.37                             | 15.136              | 9.55            | 1.59                               | 3.61                          |
| 365.3        | 0.033           | 0.37                             | 17.433              | 8.55            | 2.04                               | 3.68                          |
| 363.1        | 0.045           | 0.33                             | 10.325              | 7.77            | 1.33                               | 3.50                          |
| 363.1        | 0.050           | 0.33                             | 9.657               | 6.78            | 1.42                               | 3.47                          |
| 361.3        | 0.062           | 0.30                             | 6.098               | 6.36            | 0.96                               | 3.31                          |
| 361.3        | 0.065           | 0.30                             | 5.929               | 6.16            | 0.96                               | 3.30                          |
| 360.6        | 0.071           | 0.29                             | 4.457               | 5.90            | 0.75                               | 3.20                          |
| 360.0        | 0.081           | 0.28                             | 3.564               | 5.38            | 0.66                               | 3.11                          |
| 358.0        | 0.121           | 0.25                             | 1.370               | 3.98            | 0.34                               | 2.75                          |
| 357.9        | 0.126           | 0.25                             | 1.194               | 3.92            | 0.30                               | 2.69                          |
| 356.7        | 0.164           | 0.23                             | 0.787               | 3.16            | 0.25                               | 2.54                          |
| 356.6        | 0.172           | 0.23                             | 0.685               | 3.07            | 0.22                               | 2.48                          |
| 355.7        | 0.229           | 0.22                             | 0.672               | 2.42            | 0.28                               | 2.49                          |
| 355.0        | 0.269           | 0.21                             | 0.499               | 2.13            | 0.23                               | 2.38                          |
| 355.0        | 0.277           | 0.21                             | 0.472               | 2.07            | 0.23                               | 2.36                          |
| 352.5        | 0.591           | 0.18                             | 0.103               | 1.18            | 0.09                               | 1.76                          |

Standard uncertainties are  $u(T) = 0.2$  K,  $u(P) = 0.5$  kPa,  $u(x_{\text{Et}}) = 0.004$ .

The binary interaction parameters determined for the two subsystems are listed in Table 6, along with the respective root mean-square deviations (RMSD) for the equilibrium variables  $K_{\beta\text{d}}$ ,  $\alpha_{\beta\text{d}/\text{Et}}$  and  $\gamma_{\beta\text{d}}$ .



**Table 6.** Binary interaction parameters regressed by NRTL model and respective root mean-square deviations (RMSD) for the binaries  $\beta$ -damascenone (1) + ethanol (2) and  $\beta$ -damascenone (1) + water (3).

| Binary (i-j) | Correlation parameters <sup>a</sup>     |   | RMSD <sup>b</sup> |                              |                    |
|--------------|---|---|-------------------|------------------------------|--------------------|
|              | $A_{ij}^0/\text{J}\cdot\text{mol}^{-1}$ | $A_{ji}^0/\text{J}\cdot\text{mol}^{-1}$ | $K_{\beta d}$     | $\alpha_{\beta d/\text{Et}}$ | $\gamma_{\beta d}$ |
| (1) – (2)    | 235497.60                               | 11488.77                                | 0.95              | 0.17                         | 286.6              |
| (1) – (3)    | -1995.73                                | 31600.27                                |                   |                              |                    |

<sup>a</sup>with  $\alpha_{ij}$  set to 0.3 for the two binary systems and temperature-dependent parameters  $A_{ij}^T$  and  $A_{ji}^T/\text{J}\cdot\text{mol}^{-1}\cdot\text{K}^{-1}$  set to zero.

$${}^b\text{RMSD} = \left[ \frac{1}{N} \sum_{i=1}^N (E_{\beta d i_{\text{exp}}} - E_{\beta d i_{\text{calc}}})^2 \right]^{\frac{1}{2}}, \text{ with } E_{\beta d} \text{ representing } K_{\beta d}, \alpha_{\beta d/\text{Et}} \text{ and } \gamma_{\beta d}.$$

Figure 3 depicts the experimental partition coefficients and relative volatilities of  $\beta$ -damascenone in terms of the ethanol mole fraction of the boiling liquid, along with NRTL correlations. Overall, the experimental data are well correlated by the NRTL model for the entire temperature range. For ethanol mole fractions at which  $K_{\beta d} > 1$ , as denoted by the dashed line in Figure 3, the concentrations of  $\beta$ -damascenone are higher in the vapor phase than in the liquid phase. Analogously, at the region where  $\alpha_{\beta d/\text{Et}} > 1$  the compound is more volatile than ethanol. As observed in the figure,  $\beta$ -damascenone is more concentrated in the vapor phase for  $x_{\text{Et}} < 0.15$ , becoming more volatile than ethanol when  $x_{\text{Et}} < 0.06$ . This is reflected in the absolute and relative volatilities of  $\beta$ -damascenone, which increase substantially with decreasing ethanol mole fractions, reaching maximum predicted values of 65.2 and 5.43 for  $K_{\beta d}$  and  $\alpha_{\beta d/\text{Et}}$ , respectively. This high volatility in the water-rich region is accompanied by high activity coefficients (Table 5), which indicate that deviations from ideality in this region are quite pronounced. As ethanol concentration in the liquid phase further increases, values of  $K_{\beta d}$  decrease over 400 times, reaching 0.10 when  $x_{\text{Et}} = 0.59$ .

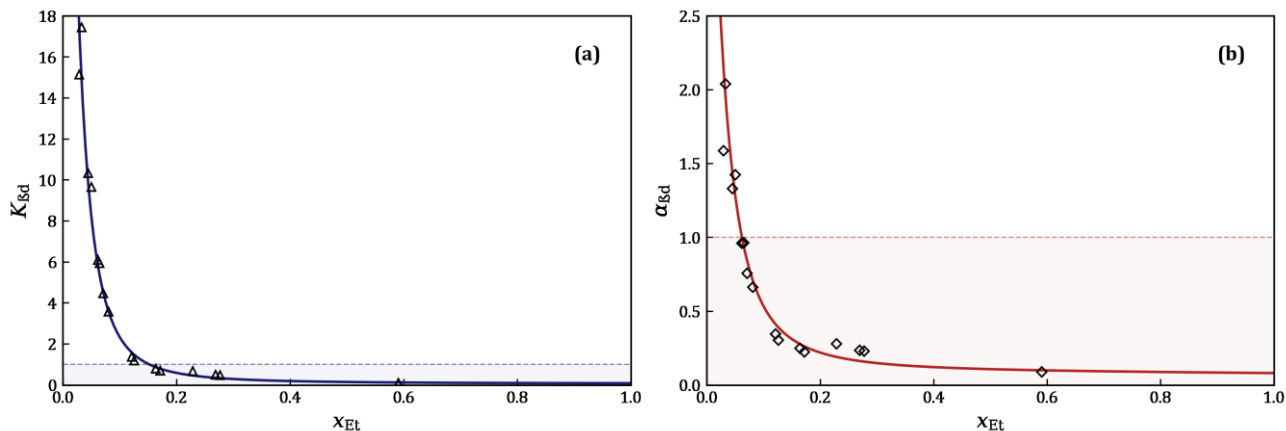


**Figure 3.** Evolution of (a) the absolute volatility ( $K_{\beta_d}$ ) and (b) the relative volatility ( $\alpha_{\beta_d/Et}$ ) of  $\beta$ -damascenone as a function of ethanol mole fraction in the liquid phase ( $x_{Et}$ ):  $\Delta$ , experimental  $K_{\beta_d}$  data; — (solid blue line), NRTL correlation for  $K_{\beta_d}$ ;  $\diamond$ , experimental  $\alpha_{\beta_d/Et}$  data; — (solid orange line), NRTL correlation for  $\alpha_{\beta_d/Et}$ .

The behavior observed for  $\beta$ -damascenone can be explained by two main factors: [1] the higher solubility of most aroma compounds in ethanol than in water, which reduces their concentration in the headspace above solutions that are richer in ethanol; [2] the relatively high hydrophobicity of  $\beta$ -damascenone, conveyed by a  $\log K_{ow}$  of 4.20. This high hydrophobicity results in the aroma compound preferably positioning itself with ethanol in the interfacial layer between the aqueous liquid and the headspace, being more prone to evaporation, especially when lower amounts of ethanol are present at the interface<sup>6,63</sup>. Furthermore, the distribution of  $\beta$ -damascenone between the coexisting vapor and liquid phases at different ethanol compositions is modulated by physicochemical effects involving structural changes associated with the ethanol-water matrix. When small amounts of ethanol are present in aqueous solutions ( $x_{Et} < 0.05$ ), the ethanol molecules tend to be monodispersed within the hydrogen bonded networks formed by water molecules<sup>64,65</sup>. As the solution becomes richer in ethanol, ethanol molecules begin to aggregate to form micelle-like structures that could entrap hydrophobic aroma molecules, thus limiting their release into the headspace<sup>66</sup>. This could explain the trend observed in Figure 3.

### 3.2. Batch distillation and process simulation

The results for the experimental batch distillation are depicted in Figure 4 as hollow shapes. Figure 4(a) shows the mass concentration profiles of ethanol and  $\beta$ -damascenone throughout

distillation. As can be observed in the figure, from the beginning of the sampling stage and up until 90 min of distillation, the ethanol concentration in the distillate is maintained at roughly  $0.9 \text{ g}\cdot\text{g}^{-1}$ ; at such concentrations,  $\beta$ -damascenone is less volatile than ethanol and is mostly refluxed into the reboiler. Even if small amounts of  $\beta$ -damascenone can pass into the distillate at this point, its concentrations in the samples are below detection limits of the chromatographic method employed in this work. Once the column is gradually depleted of ethanol, the relative volatility of  $\beta$ -damascenone increases and the compound passes into the distillate, reaching a concentration peak at  $w_{\text{Et}} \approx 0.5 \text{ g}\cdot\text{g}^{-1}$ . Approximately 99% of the initial mass of ethanol in the reboiler was recovered in the distillate by the end of the distillation process. The total cumulated mass of ethanol is presented in Figure 4(b) and the temperature variations in the reboiler over time are depicted in Figure 4(c). The temperature initially increases as the liquid is brought to a boil and the column plates are gradually filled. The subsequent stage is characterized by nearly constant temperatures as the column is operated in total reflux and some of the  $\beta$ -damascenone and water in the plates is refluxed back to the reboiler. Slight increases in temperature are observed as the distillate begins to be collected and a gradient of ethanol is formed within the column. The temperature in the reboiler continues to rise while the boiling liquid is depleted of ethanol and  $\beta$ -damascenone, reaching a final plateau after 120 min, when the reboiler is depleted of ethanol and  $\beta$ -damascenone.

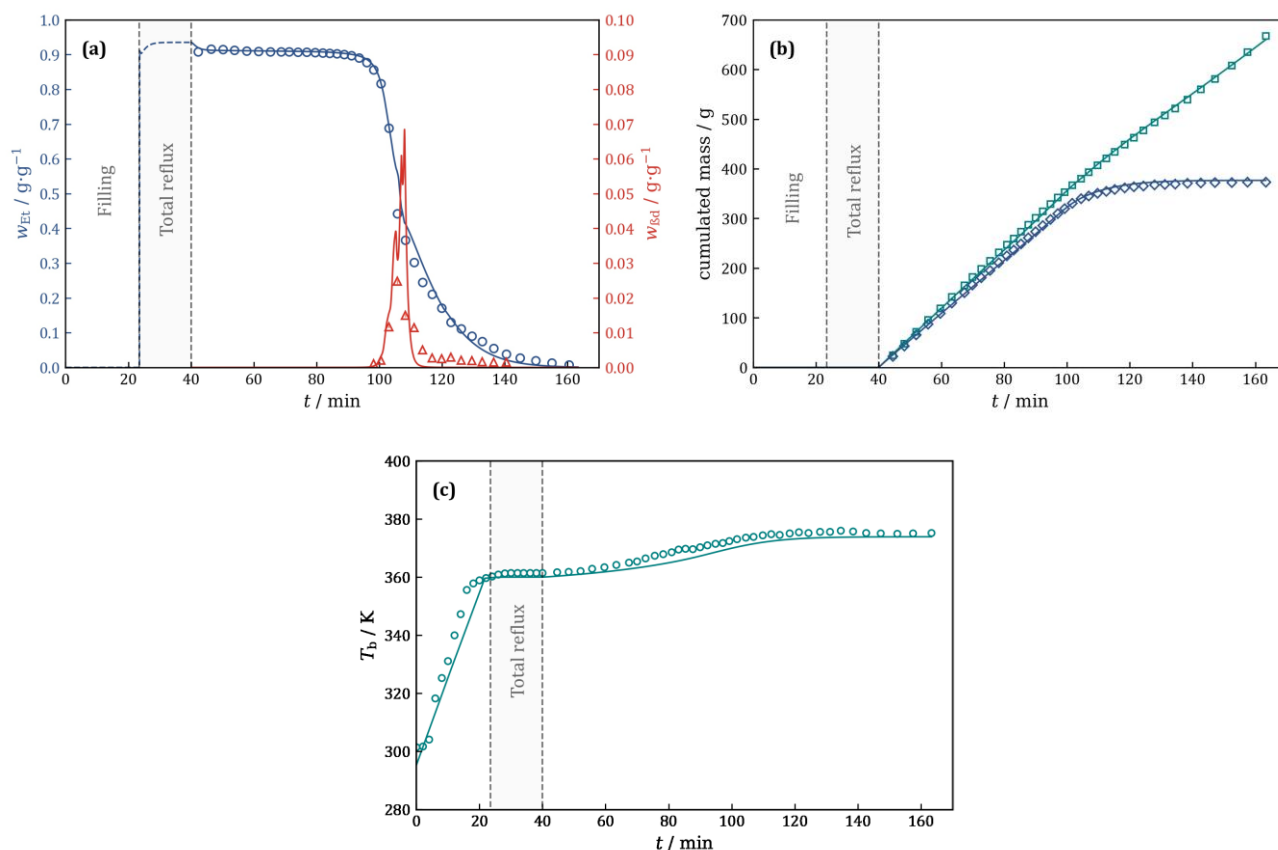


**Figure 4.** Experimental and simulated data for the batch distillation of a model solution consisting of  $\beta$ -damascenone, ethanol and water. (a) mass concentration profiles of ( $\circ$ ) ethanol and ( $\Delta$ )  $\beta$ -damascenone in the distillate, (b) cumulated masses of ( $\square$ ) distillate and of ( $\diamond$ ) ethanol as a function of time and (c) ( $\circ$ ) evolution of the temperature in the reboiler over time. — (solid lines), data simulated with BatchColumn (ProSim SA, France) using the binary NRTL coefficients determined in this work.

Based on these results, a simulation module was built to represent the experimental distillation and validate the NRTL parameters determined in this work for  $\beta$ -damascenone in ethanol-water mixtures. The simulations were adjusted to the experimental data for water and ethanol, which are the major compounds. The variables considered in the adjustment include the cumulated mass of distillate, the cumulated mass of ethanol distilled and the mass concentration of ethanol in the distillate. The efficacy of the column plates in the simulation module was determined as the value that allowed to achieve the best fit with the experimental ethanol composition in the distillate after running different simulations with efficacies between 0.5 and 1.0. Liquid holdup in the plates was estimated from the experimental distillation based on the height of the liquid observed in the column plates and the plate diameter. Simulation parameters are given in Table 7. The distillation stage was

divided in four theoretical distillation stages in the simulation module to integrate the variations in heat losses over time and thus achieve a better adjustment with the experimental data. The condenser was regarded as a total condenser and the liquid in the reboiler was considered to remain a homogeneous mixture throughout distillation.

**Table 7.** Input parameters of the simulation module.

| <b>Simulation specifications</b> |       |     |
|----------------------------------|-------|-----|
| Number of trays                  | 12    |     |
| Efficiency                       |       |     |
| Trays 2-11                       | 0.75  |     |
| Reboiler                         | 1.00  |     |
| Condenser                        | 1.00  |     |
| Liquid holdup                    |       |     |
| Trays 2-11                       | 3     | mL  |
| Condenser                        | 5     | mL  |
| Pressure <sup>a</sup>            |       |     |
| Condenser                        | 103.0 | kPa |
| Pressure loss                    | 0.8   | kPa |

<sup>a</sup>as measured during the experimental distillation.

The solid lines in Figure 4 depict the simulated mass concentration profiles of ethanol and  $\beta$ -damascenone in the distillate ( $w_{Et}$  and  $w_{\beta d}$ , respectively) and the cumulated masses of distillate and of ethanol. In Figure 4(a), a dashed blue line was added to represent ethanol mass fraction in the condenser during the filling and total reflux stages. Given the gradual increase of ethanol mass concentration within the column in the filling stage, the first vapors reach the condenser with a high ethanol concentration, which remains nearly constant during the total reflux stage. As observed in the figure, the experimental data are overall well represented by the simulation module. Minor discrepancies can be observed in Figure 4(a) near the concentration peak of  $\beta$ -damascenone, where concentrations for both  $\beta$ -damascenone and ethanol seem to be overestimated by the simulation. Since ethanol concentrations in the distillate undergo a steep decrease in the region, the peak of  $\beta$ -damascenone rises rather swiftly and only a limited amount data points were collected in the

zone. Furthermore, the experimental concentrations of  $\beta$ -damascenone are higher than the simulated values for the last 50 min of distillation. It is possible that small amounts of the compound were retained on the walls between the reflux valve and the cooler throughout distillation. If this was the case, as the distillate became increasingly aqueous and the liquid flowed at a slower rate, the  $\beta$ -damascenone retained could have been carried by the distillate into the samples. Nevertheless, the concentration profile of  $\beta$ -damascenone is sufficiently well represented to consider that the NRTL parameters determined in this work would allow to correctly simulate its behavior during a spirit distillation.

Figure 5 presents the evolution of the liquid and vapor compositions and the temperature throughout the column at different distillation times of the computer simulation: (a) 24'50'', (b) 40'00'', (c) 90'00'' and (d) 110'00''. Stages 1 and 12 correspond to the condenser and the reboiler, respectively, and stages 2 to 11 correspond to the 10 column plates. Fig. 5(a) represents the beginning of the total reflux period, when a gradient of decreasing ethanol concentration and increasing temperature can be observed from the condenser and upper stages to the reboiler; at this point,  $\beta$ -damascenone has begun to rise into the bottom of the column, propelled by the low ethanol concentrations in the reboiler and in the lower stages. By the end of the period in which the column operates at total reflux (Fig. 5(b)), the column plates are highly concentrated in ethanol, prompting most of the  $\beta$ -damascenone to be refluxed into the reboiler. A steep increase in concentration for  $\beta$ -damascenone can be observed again at 90 min (Fig. 5(c)), when the ethanol and temperature gradients within the column are more pronounced and ethanol concentration in the reboiler is lower than  $0.1 \text{ g}\cdot\text{g}^{-1}$ . After another 20 min of distillation (Fig. 5(d)), the column was nearly depleted of ethanol and  $\beta$ -damascenone, and the temperature of the liquid, which is essentially governed by ethanol composition, is significantly higher.

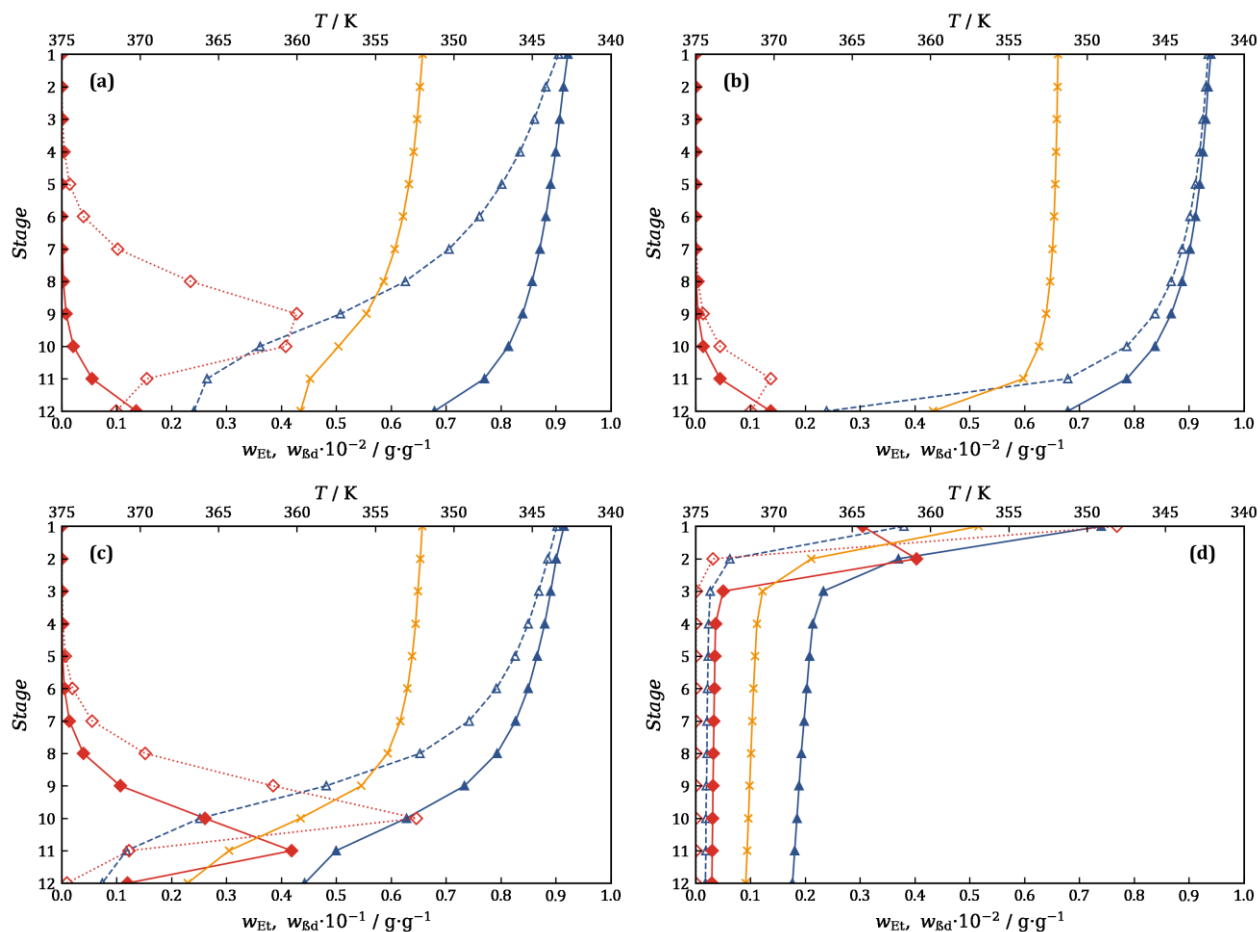


**Figure 5.** Mass concentrations of ( $\Delta$ ) ethanol and ( $\diamond$ )  $\beta$ -damascenone and ( $\times$ ) temperature variations in the liquid and the vapor in each stage at the beginning and the end of the total reflux period ((a) and (b), respectively), at the end of the plateau of ethanol mass concentration (c), and near the end of the distillation (d). Hollow symbols and dotted lines correspond to the liquid phase, whereas filled symbols and solid lines represent the vapor phase. Stages 1 and 12 correspond to the condenser and the reboiler, respectively.

#### 4. CONCLUSIONS

New VLE data were measured for  $\beta$ -damascenone highly diluted in ethanol-water mixtures using a recirculating ebulliometer at 101.3 kPa. Pure component properties for  $\beta$ -damascenone were collected from the literature and computed with predictive methods, and the compound was added to the Simulis Thermodynamics database. The new experimental data were well correlated by the NRTL model and binary interaction parameters were determined for the binaries  $\beta$ -damascenone-ethanol and  $\beta$ -damascenone-water. The applicability of the experimental data for simulation purposes was checked by simulating a

laboratory-scale batch distillation of a model solution for the ternary system. The binary NRTL parameters allowed to correctly represent the behavior of  $\beta$ -damascenone during a batch distillation and could be used to predict the behavior of the compound during an industrial-scale distillation of alcoholic beverages. This approach can be extended to other aroma compounds that play a key role in the typicality of distilled spirits.



## **AUTHOR INFORMATION**

### ***Corresponding author***

\*Gabriela Zanghelini. E-mail: [gabriela.zanghelini@agroparistech.fr](mailto:gabriela.zanghelini@agroparistech.fr)

### ***ORCID***

Gabriela Zanghelini: 0000-0001-6993-3878

Violaine Athès: 0000-0002-2194-8517

Martine Esteban-Decloux: 0000-0002-8084-2528

Pierre Giampaoli: 0000-0002-6756-0403

Stéphane Vitu: 0000-0002-5442-1279

### ***Notes***

The authors declare no competing financial interest.

### ***Funding***

This work was supported by the foundation Jean Poupelain.

### ***Acknowledgements***

The authors are thankful to Nicolas Descharles for his valuable assistance with the analytical measurements and to N'Guessan Charles Romaric Tano for his aid with distillation experiments.

## REFERENCES

- (1) Lurton, L.; Ferrari, G.; Snackers, G. Cognac: Production and Aromatic Characteristics. In *Alcoholic Beverages: Sensory Evaluation and Consumer Research*; Piggott, J. R., Ed.; Woodhead Publishing Limited: Cambridge, UK, **2012**; pp 242–266. <https://doi.org/10.1016/B978-0-85709-051-5.50011-0>.
- (2) Ammari, A.; Schroen, K. Flavor Retention and Release from Beverages: A Kinetic and Thermodynamic Perspective. *J. Agric. Food Chem.* **2018**, *66* (38), 9869–9881. <https://doi.org/10.1021/acs.jafc.8b04459>.
- (3) Styger, G.; Prior, B.; Bauer, F. F. Wine Flavor and Aroma. *J. Ind. Microbiol. Biotechnol.* **2011**, *38* (9), 1145–1159. <https://doi.org/10.1007/s10295-011-1018-4>.
- (4) Ebeler, S. E.; Thorngate, J. H. Wine Chemistry and Flavor: Looking into the Crystal Glass. *J. Agric. Food Chem.* **2009**, *57* (18), 8098–8108. <https://doi.org/10.1021/jf9000555>.
- (5) Buttery, R. G.; Teranishi, R.; Ling, L. C.; Turnbaugh, J. G. Quantitative and Sensory Studies on Tomato Paste Volatiles. *J. Agric. Food Chem.* **1990**, *38* (1), 336–340. <https://doi.org/10.1021/jf00091a074>.
- (6) Ickes, C. M.; Cadwallader, K. R. Effects of Ethanol on Flavor Perception in Alcoholic Beverages. *Chemosens. Percept.* **2017**, *10* (4), 119–134. <https://doi.org/10.1007/s12078-017-9238-2>.
- (7) Pineau, B.; Barbe, J. C.; Van Leeuwen, C.; Dubourdieu, D. Which Impact for  $\beta$ -Damascenone on Red Wines Aroma? *J. Agric. Food Chem.* **2007**, *55* (10), 4103–4108. <https://doi.org/10.1021/jf070120r>.
- (8) Masuda, M.; Nishimura, K.-I.-C. Occurrence and Formation of Damascenone, Trans-2,6,6-Trimethyl-1-Crotonyl-Cyclohexa-1,3-Diene, in Alcoholic Beverages. *J. Food Sci.* **1980**, *45* (2), 396–397. <https://doi.org/10.1111/j.1365-2621.1980.tb02626.x>.
- (9) Sefton, M. A.; Skouroumounis, G. K.; Elsey, G. M.; Taylor, D. K. Occurrence, Sensory Impact, Formation, and Fate of Damascenone in Grapes, Wines, and Other

- Foods and Beverages. *J. Agric. Food Chem.* **2011**, *59* (18), 9717–9746. <https://doi.org/10.1021/jf201450q>.
- (10) Zierer, B.; Schieberle, P.; Granvogl, M. Aroma-Active Compounds in Bartlett Pears and Their Changes during the Manufacturing Process of Bartlett Pear Brandy. *J. Agric. Food Chem.* **2016**, *64* (50), 9515–9522. <https://doi.org/10.1021/acs.jafc.6b04612>.
- (11) Schreier, P.; Drawert, F.; Schmid, M. Changes in the Composition of Neutral Volatile Components during the Production of Apple Brandy. *J. Sci. Food Agric.* **1978**, *29* (8), 728–736. <https://doi.org/10.1002/jsfa.2740290811>.
- (12) Kotseridis, Y.; Baumes, R. L.; Skouroumounis, G. K. Quantitative Determination of Free and Hydrolytically Liberated  $\beta$ -Damascenone in Red Grapes and Wines Using a Stable Isotope Dilution Assay. *J. Chromatogr. A* **1999**, *849* (1), 245–254. [https://doi.org/10.1016/S0021-9673\(99\)00540-3](https://doi.org/10.1016/S0021-9673(99)00540-3).
- (13) Franitza, L.; Granvogl, M.; Schieberle, P. Influence of the Production Process on the Key Aroma Compounds of Rum: From Molasses to the Spirit. *J. Agric. Food Chem.* **2016**, *64* (47), 9041–9053. <https://doi.org/10.1021/acs.jafc.6b04046>.
- (14) Awad, P.; Athès, V.; Decloux, M. E.; Ferrari, G.; Snakkers, G.; Raguenaud, P.; Giampaoli, P. Evolution of Volatile Compounds during the Distillation of Cognac Spirit. *J. Agric. Food Chem.* **2017**, *65* (35), 7736–7748. <https://doi.org/10.1021/acs.jafc.7b02406>.
- (15) Franitza, L.; Granvogl, M.; Schieberle, P. Characterization of the Key Aroma Compounds in Two Commercial Rums by Means of the Sensomics Approach. *J. Agric. Food Chem.* **2016**, *64* (3), 637–645. <https://doi.org/10.1021/acs.jafc.5b05426>.
- (16) Pino, J. A.; Tolle, S.; Gök, R.; Winterhalter, P. Characterisation of Odour-Active Compounds in Aged Rum. *Food Chem.* **2012**, *132* (3), 1436–1441. <https://doi.org/10.1016/j.foodchem.2011.11.133>.
- (17) Genovese, A.; Ugliano, M.; Pessina, R.; Gambuti, A.; Piombino, P.; Moio, L. Comparison of the Aroma Compounds in Apricot (*Prunus Armeniaca*, L. Cv. Pellecchiella) and Apple (*Malus Pumila*, L. Cv. Annurca) Raw Distillates. *Ital. J. Food*

- Sci.* **2004**, *16* (2), 185–196.
- (18) Xiang, X. F.; Lan, Y. Bin; Gao, X. T.; Xie, H.; An, Z. Y.; Lv, Z. H.; Yin-Shi; Duan, C. Q.; Wu, G. F. Characterization of Odor-Active Compounds in the Head, Heart, and Tail Fractions of Freshly Distilled Spirit from Spine Grape (*Vitis Davidii* Foex) Wine by Gas Chromatography-Olfactometry and Gas Chromatography-Mass Spectrometry. *Food Res. Int.* **2020**, *137* (May), 109388. <https://doi.org/10.1016/j.foodres.2020.109388>.
- (19) Poisson, L.; Schieberle, P. Characterization of the Key Aroma Compounds in an American Bourbon Whisky by Quantitative Measurements, Aroma Recombination, and Omission Studies. *J. Agric. Food Chem.* **2008**, *56* (14), 5820–5826. <https://doi.org/10.1021/jf800383v>.
- (20) González-Robles, I. W.; Cook, D. J. The Impact of Maturation on Concentrations of Key Odour Active Compounds Which Determine the Aroma of Tequila. *J. Inst. Brew.* **2016**, *122* (3), 369–380. <https://doi.org/10.1002/jib.333>.
- (21) Lahne, J.; Cadwallader, K. Streamlined Analysis of Potent Odorants in Distilled Alcoholic Beverages: The Case of Tequila. *ACS Symp. Ser.* **2012**, *1104*, 37–53. <https://doi.org/10.1021/bk-2012-1104.ch003>.
- (22) de Souza, M. D. C. A.; Vásquez, P.; del Mastro, N. L.; Acree, T. E.; Lavin, E. H. Characterization of Cachaça and Rum Aroma. *J. Agric. Food Chem.* **2006**, *54* (2), 485–488. <https://doi.org/10.1021/jf0511190>.
- (23) Uselmann, V.; Schieberle, P. Decoding the Combinatorial Aroma Code of a Commercial Cognac by Application of the Sensomics Concept and First Insights into Differences from a German Brandy. *J. Agric. Food Chem.* **2015**, *63* (7), 1948–1956. <https://doi.org/10.1021/jf506307x>.
- (24) Ferrari, G.; Lablanquie, O.; Cantagrel, R.; Ledauphin, J.; Payot, T.; Fournier, N.; Guichard, E. Determination of Key Odorant Compounds in Freshly Distilled Cognac Using GC-O, GC-MS, and Sensory Evaluation. *J. Agric. Food Chem.* **2004**, *52* (18), 5670–5676. <https://doi.org/10.1021/jf049512d>.

- (25) Ledauphin, J.; Guichard, H.; Saint-Clair, J.-F.; Picoche, B.; Barillier, D. Chemical and Sensorial Aroma Characterization of Freshly Distilled Calvados. 2. Identification of Volatile Compounds and Key Odorants. *J. Agric. Food Chem.* **2003**, *51* (2), 433–442. <https://doi.org/10.1021/jf020373e>.
- (26) Escudero, A.; Campo, E.; Fariña, L.; Cacho, J.; Ferreira, V. Analytical Characterization of the Aroma of Five Premium Red Wines. Insights into the Role of Odor Families and the Concept of Fruitiness of Wines. *J. Agric. Food Chem.* **2007**, *55* (11), 4501–4510. <https://doi.org/10.1021/jf0636418>.
- (27) Thibaud, F.; Courregelongue, M.; Darriet, P. Contribution of Volatile Odorous Terpenoid Compounds to Aged Cognac Spirits Aroma in a Context of Multicomponent Odor Mixtures. *J. Agric. Food Chem.* **2020**, *68* (47), 13310–13318. <https://doi.org/10.1021/acs.jafc.9b06656>.
- (28) Batista, F. R. M.; Meirelles, A. J. A. Computer Simulation Applied to Studying Continuous Spirit Distillation and Product Quality Control. *Food Control* **2011**, *22* (10), 1592–1603. <https://doi.org/10.1016/j.foodcont.2011.03.015>.
- (29) Decloux, M.; Coustel, J. Simulation of a Neutral Spirit Production Plant Using Beer Distillation. *Int. Sugar J.* **2005**, *107* (1283), 628–643.
- (30) Valderrama, J. O.; Toselli, L. A.; Faúndez, C. A. Advances on Modeling and Simulation of Alcoholic Distillation. Part 2: Process Simulation. *Food Bioprod. Process.* **2012**, *90* (4), 832–840. <https://doi.org/10.1016/j.fbp.2012.04.003>.
- (31) Batista, F. R. M.; Follegatti-romero, L. A.; Meirelles, A. J. A. A New Distillation Plant for Neutral Alcohol Production. *Sep. Purif. Technol.* **2013**, *118*, 784–793. <https://doi.org/10.1016/j.seppur.2013.08.030>.
- (32) Esteban-Decloux, M.; Deterre, S.; Kadir, S.; Giampaoli, P.; Albet, J.; Joulia, X.; Baudouin, O. Two Industrial Examples of Coupling Experiments and Simulations for Increasing Quality and Yield of Distilled Beverages. *Food Bioprod. Process.* **2014**, *92* (4), 343–354. <https://doi.org/10.1016/j.fbp.2013.10.001>.
- (33) Puentes, C.; Joulia, X.; Vidal, J. P.; Esteban-Decloux, M. Simulation of Spirits

- Distillation for a Better Understanding of Volatile Aroma Compounds Behavior: Application to Armagnac Production. *Food Bioprod. Process.* **2018**, *112*, 31–62. <https://doi.org/10.1016/j.fbp.2018.08.010>.
- (34) Gaiser, M.; Bell, G. M.; Lim, A. W.; Roberts, N. A.; Faraday, D. B. F.; Schulz, R. A.; Grob, R. Computer Simulation of a Continuous Whisky Still. *J. Food Eng.* **2002**, *51* (1), 27–31. [https://doi.org/10.1016/S0260-8774\(01\)00033-4](https://doi.org/10.1016/S0260-8774(01)00033-4).
- (35) Douady, A.; Puentes, C.; Awad, P.; Esteban-Decloux, M. Batch Distillation of Spirits: Experimental Study and Simulation of the Behaviour of Volatile Aroma Compounds. *J. Inst. Brew.* **2019**, *125* (2), 268–283. <https://doi.org/10.1002/jib.560>.
- (36) Scanavini, H. F. A.; Ceriani, R.; Cassini, C. E. B.; Souza, E. L. R.; Maugeri Filho, F.; Meirelles, A. J. A. Cachaça Production in a Lab-Scale Alembic: Modeling and Computational Simulation. *J. Food Process Eng.* **2010**, *33* (SUPPL. 1), 226–252. <https://doi.org/10.1111/j.1745-4530.2008.00352.x>.
- (37) Scanavini, H. F. A.; Ceriani, R.; Meirelles, A. J. A. Cachaça Distillation Investigated on the Basis of Model Systems. *Brazilian J. Chem. Eng.* **2012**, *29* (2), 429–440. <https://doi.org/10.1590/S0104-66322012000200022>.
- (38) Soares, A. M.; Henderson, N.; Mota, B. T.; Pires, A. P.; Ramos, V. D. A New Pot Still Distillation Model Approach with Parameter Estimation by Multi-Objective Optimization. *Comput. Chem. Eng.* **2019**, *130*, 106570. <https://doi.org/10.1016/j.compchemeng.2019.106570>.
- (39) Sacher, J.; García-Llobodanin, L.; López, F.; Segura, H.; Pérez-Correa, J. R. Dynamic Modeling and Simulation of an Alembic Pear Wine Distillation. *Food Bioprod. Process.* **2013**, *91* (4), 447–456. <https://doi.org/10.1016/j.fbp.2013.04.001>.
- (40) Claus, M. J.; Berglund, K. A. Defining Still Parameters Using CHEMCAD Batch Distillation Model for Modeling Fruit Spirits Distillations. *J. Food Process Eng.* **2009**, *32* (6), 881–892. <https://doi.org/10.1111/j.1745-4530.2008.00251.x>.
- (41) Kontogeorgis, G. M.; Dohrn, R.; Economou, I. G.; De Hemptinne, J. C.; Kate, A.; Kuitunen, S.; Mooijer, M.; Zilnik, L. F.; Vesovic, V. Industrial Requirements for

- Thermodynamic and Transport Properties: 2020. *Ind. Eng. Chem. Res.* **2021**, *60* (13), 4987–5013. <https://doi.org/10.1021/acs.iecr.0c05356>.
- (42) Fingerhut, R.; Chen, W. L.; Schedemann, A.; Cordes, W.; Rarey, J.; Hsieh, C. M.; Vrabec, J.; Lin, S. T. Comprehensive Assessment of COSMO-SAC Models for Predictions of Fluid-Phase Equilibria. *Ind. Eng. Chem. Res.* **2017**, *56* (35), 9868–9884. <https://doi.org/10.1021/acs.iecr.7b01360>.
- (43) Gmehling, J.; Li, J.; Schiller, M. A Modified UNIFAC Model. 2. Present Parameter Matrix and Results for Different Thermodynamic Properties. *Ind. Eng. Chem. Res.* **1993**, *32* (1), 178–193. <https://doi.org/10.1021/ie00013a024>.
- (44) Fonseca, L. A. A. P.; Sartoratto, A.; Cremasco, M. A. Experimental Determination of Thermodynamic Properties of Terpene and Aromatic Ketones by Gas Chromatography. *J. Mol. Liq.* **2021**, *322* (October), 114531. <https://doi.org/10.1016/j.molliq.2020.114531>.
- (45) Arce, A.; Arce, A.; Martínez-Ageitos, J. M.; Soto, A. Isobaric Vapor–Liquid Equilibria of 1,1-Dimethylethoxy-Butane+methanol or Ethanol+water at 101.32kPa. *Fluid Phase Equilib.* **2007**, *259* (1), 57–65. <https://doi.org/10.1016/j.fluid.2007.01.038>.
- (46) Kamihama, N.; Matsuda, H.; Kurihara, K.; Tochigi, K.; Oba, S. Isobaric Vapor–Liquid Equilibria for Ethanol + Water + Ethylene Glycol and Its Constituent Three Binary Systems. *J. Chem. Eng. Data* **2012**, *57* (2), 339–344. <https://doi.org/10.1021/je2008704>.
- (47) Riddick, J. A.; Bunger, W. B.; Sakano, T. K. *Organic Solvents: Physical Properties and Methods of Purification*, 4th editio.; Wiley: New York, 1986.
- (48) S.R.C. PhysProp Database. U.S. Environmental Protection Agency.
- (49) Hansch, C.; Leo, A.; Hoekman, D. H. *Exploring QSAR. Hydrophobic, Electronic, and Steric Constants*; American Chemical Society: Washington, DC, 1995.
- (50) ProSim S.A. Simulis Thermodynamics. Labège, France 2021.
- (51) Nelson, C. Investigation of Vaporization Enthalpies and Vapor Pressures of Organic

- Compounds by Correlation Gas Chromatography, University of Missouri, St. Louis, 2018.
- (52) Koretsky, M. D. *Engineering and Chemical Thermodynamics*, 2nd ed.; John Wiley & Sons, 2013.
- (53) Joback, K. G.; Reid, R. C. Estimation of Pure-Component Properties from Group-Contributions. *Chem. Eng. Commun.* **1987**, *57* (1–6), 233–243. <https://doi.org/10.1080/00986448708960487>.
- (54) Zanghelini, G.; Athès, V.; Esteban-Decloux, M.; Giampaoli, P.; Vitu, S. Isobaric Vapour-Liquid Equilibrium of  $\alpha$ -Terpineol Highly Diluted in Hydroalcoholic Mixtures at 101.3 KPa: Experimental Measurements and Thermodynamic Modeling. *J. Chem. Thermodyn.* **2022**, *171*, 106806. <https://doi.org/10.1016/j.jct.2022.106806>.
- (55) *International Alcoholometric Tables, OIML R22*; International Organisation of Legal Metrology: [https://www.oiml.org/en/files/pdf\\_r/r022-e75.pdf](https://www.oiml.org/en/files/pdf_r/r022-e75.pdf), 1975.
- (56) JCGM. *Evaluation of Measurement Data — Guide to the Expression of Uncertainty in Measurement*; JCGM 100:2008 (GUM 1995 with minor corrections); Joint Committee for Guides in Metrology, 2008.
- (57) Taylor, B. N.; Kuyatt, C. E. *Guidelines for Evaluating and Expressing the Uncertainty of NIST Measurement Results*; NIST Tech. Note 1297; National Institute of Standards and Technology: Gaithersburg, MD, 1994.
- (58) Raal, J. D.; Ramjugernath, D. Rigorous Characterization of Static and Dynamic Apparatus for Measuring Limiting Activity Coefficients. *Fluid Phase Equilib.* **2001**, *187–188*, 473–487. [https://doi.org/10.1016/S0378-3812\(01\)00567-2](https://doi.org/10.1016/S0378-3812(01)00567-2).
- (59) Valderrama, J. O.; Faúndez, C. A.; Toselli, L. A. Advances on Modeling and Simulation of Alcoholic Distillation. Part 1: Thermodynamic Modeling. *Food Bioprod. Process.* **2012**, *90* (4), 819–831. <https://doi.org/10.1016/j.fbp.2012.04.004>.
- (60) Puentes, C.; Joulia, X.; Athès, V.; Esteban-Decloux, M. Review and Thermodynamic Modeling with NRTL Model of Vapor-Liquid Equilibria (VLE) of Aroma



- Compounds Highly Diluted in Ethanol-Water Mixtures at 101.3 KPa. *Ind. Eng. Chem. Res.* **2018**, *57* (10), 3443–3470. <https://doi.org/10.1021/acs.iecr.7b03857>.
- (61) Faúndez, C. A.; Alvarez, V. H.; Valderrama, J. O. Phase Equilibrium in Binary Aqueous Mixtures of Interest in Alcoholic Distillation Using a Modified PSRK Equation of State. *J. Phase Equilibria Diffus.* **2004**, *25* (3), 230–236. <https://doi.org/10.1361/15477030419487>.
- (62) Renon, H.; Prausnitz, J. M. Local Compositions in Thermodynamic Excess Functions for Liquid Mixtures. *AIChE J.* **1968**, *14* (1), 135–144. <https://doi.org/10.1002/aic.690140124>.
- (63) Tsachaki, M.; Aznar, M.; Linforth, R. S. T.; Taylor, A. J. Dynamics of Flavour Release from Ethanolic Solutions. *Dev. Food Sci.* **2006**, *43* (C), 441–444. [https://doi.org/10.1016/S0167-4501\(06\)80104-4](https://doi.org/10.1016/S0167-4501(06)80104-4).
- (64) Conner, J. M.; Birkmyre, L.; Paterson, A.; Piggott, J. R. Headspace Concentrations of Ethyl Esters at Different Alcoholic Strengths. *J. Sci. Food Agric.* **1998**, *77* (1), 121–126. [https://doi.org/10.1002/\(SICI\)1097-0010\(199805\)77:1<121::AID-JSFA14>3.0.CO;2-V](https://doi.org/10.1002/(SICI)1097-0010(199805)77:1<121::AID-JSFA14>3.0.CO;2-V).
- (65) D'Angelo, M.; Onori, G.; Santucci, A. Self-Association Behaviour of Alcohols in Diluted Aqueous Solutions (\*). *Nuovo Cim. D* **1994**, *16* (9), 1499–1514. <https://doi.org/10.1007%2FBBF02462035>.
- (66) Onori, G.; Santucci, A. Dynamical and Structural Properties of Water/Alcohol Mixtures. *J. Mol. Liq.* **1996**, *69* (9 SPEC. ISS.), 161–181. [https://doi.org/10.1016/S0167-7322\(96\)90012-4](https://doi.org/10.1016/S0167-7322(96)90012-4).